Inorganic Chemistry

Article

Forcing Dicyanamide Coordination to f-Elements by Dissolution in Dicyanamide-Based Ionic Liquids

Si-Fu Tang, Volodymyr Smetana, Manish Kumar Mishra, Steven P. Kelley, Olivier Renier, Robin D. Rogers,* and Anja-Verena Mudring*

Read Online

ACCESS | Metrics & More | Article Recommendations | Supporting Information

ABSTRACT: A robust general route to lanthanide dicyanamide (DCA$^-$) complexes has been developed where f-element salts are dissolved in DCA$^-$-based ionic liquids (ILs) directly or formed *in situ*, forcing coordination of these normally weakly coordinating soft N-donor anions, even in an ambient, non-moisture-excluding environment. A series of lanthanide complexes [C$_2$mim][Ln(DCA)$_4$(H$_2$O)$_4$] (C$_2$mim = 1-ethyl-3-methylimidazolium; Ln = La, Nd, Eu, Tb, Dy, and Yb) and [C$_2$mim]$_{3n}$[La(OH$_2$)$_4$(μ^2-DCA)$_4$]$_n$[La(OH$_2$)$_2$(μ^3-DCA)$_3$(μ^2-DCA)$_4$]$_{2n}$(Cl)$_{4n}$ were crystallized under a variety of conditions using this methodology and structurally characterized using single crystal X-ray diffraction. Although not all examples were isostructural, the dominant feature across the series was the presence of [Ln(DCA)$_4$(H$_2$O)$_4$]$^-$ anionic nodes with all terminal DCA$^-$ ligands accepting hydrogen bonds from the coordinated water molecules forming a 3D metal organic framework. To determine if any structural clues might aid in the further development of the synthetic methodology, the metal-free IL [C$_1$mim][DCA] (C$_1$mim = 1,3-dimethylimidazolium), a room-temperature solid, crystalline analogue of the reaction IL, which is liquid at room temperature, was also prepared and structurally characterized. The ready isolation of these compounds allowed us to begin an investigation of the physical properties such as the luminescence at room and low temperatures for the Eu, Tb, and Dy representatives.
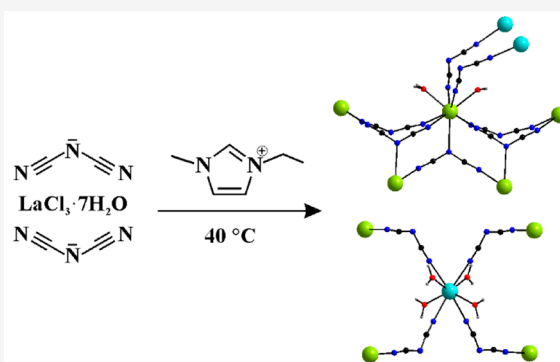
INTRODUCTION

The field of ionic liquids (ILs) has undergone rapid development in recent years.[1] It is well-known that ILs can feature unique properties, such as a negligible vapor pressure, a wide liquidus range, a comparably good thermal stability, and a wide electrochemical window, which are all advantageous for various applications.[2−10] As an important branch, metal-containing ILs, especially lanthanide-containing ILs (or lanthanide-doped ILs), are attracting more and more attention.[11−20] The interest mainly arises from the consideration that metal-containing ILs can possess not only the merits of ILs but also those of the metals incorporated in the ILs.[11] Through the introduction of lanthanide elements, ILs can be endowed with new and interesting properties, such as luminescence[11−19] and magnetism.[12]

It is possible to make lanthanide-based ILs, and some prominent examples are the europium-containing ILs with a general formula [R]$_x$[Eu(Tf$_2$N)$_{3+x}$] [Tf$_2$N = bis(trifluoromethanesulfonyl)amide; x = 1 for R = 1-propyl-3-methylimidazolium (C$_3$mim) and 1-butyl-3-methylimidazolium (C$_4$mim); x = 2 for R = 1-butyl-1-methylpyrrolidinium (C$_4$mpyr)].[13] These Eu-containing ILs do not contain any water or other neutral ligands. It was found that they all melt below 100 °C and show strong red emission, good color purity,

and long decay times. Using a similar concept, homoleptic triflates could be obtained and characterized.[21] Rare earth triflates dissolved in ILs are interesting as catalysts for a variety of organic reactions.[11,22] However, in order to obtain anhydrous, and even more challenging, homoleptic complexes, such compounds have to be made under strictly inert conditions, taking the relative Lewis basicities into account.[23]

Lanthanide cations are generally quite oxophilic, and whenever water, or even humidity from the air, is present, it is difficult to avoid the formation of the fully hydrated species [Ln(H$_2$O)$_8$]$^{3+}$ or [Ln(H$_2$O)$_9$]$^{3+}$, depending on the size of the lanthanide ion. ILs as solvents offer an interesting aspect, as they allow otherwise unattainable water-poor coordination environments to be obtained for the lanthanides.[24,25] This is of interest as water may have a significant effect on the properties of ILs, not only the viscosity, decomposition temperature, or the melting point, but also on other physicochemical
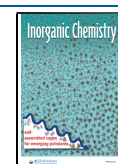
properties as thiocyanate-based, lanthanide-containing ILs- $[C_4mim]_{x-3}[Ln(NCS)_x(H_2O)_y]$ (x = 6−8; y = 0−2; Ln = Y, La, Pr, Nd, Sm, Eu, Gd, Tb, Ho, Er, and Yb) have low melting points that can be altered by changing the water contents in the complex anion.[26] These lanthanide-containing ILs exhibit good solubility in nonpolar solvents, are miscible with other ILs, and are interesting candidates for catalytic and spectroscopic applications. The dysprosium analogues, $[C_6mim]_{5-x}[Dy(SCN)_{8-x}(H_2O)_x]$ (x = 0−2, C_6mim = 1-hexyl-3-methylimidazolium), exhibit a strong response to external magnetic fields, and their luminescence properties strongly depend on the water content.[12] However, when designing luminescent ILs based on lanthanides, water can often be a trade-off. On one hand, the absence of water yields highly luminescent materials, but on the other the melting point of such materials is frequently higher.[27] Thus, a careful balance needs to be attained.

In order to expand the range of lanthanide-containing ILs, we need to explore other interesting, typically weakly N-donor coordinating ions such as dicyanamide ($N(CN)_2^-$ or DCA$^-$). DCA$^-$ ILs are typically characterized by a low viscosity.[28,29] Hydrophobic DCA$^-$ ILs have been shown to be useful in the extraction of transition metal cations.[30] Metal complexes of dicyanamide ions usually possess intriguing optical, magnetic, and electronic properties, since the quasi-π-conjugated dicyanamide ligands serve as an effective mediator to transmit magnetic and electronic interactions.[31] Such lanthanide complexes are also relevant to understanding the challenging separation chemistry of trivalent actinides and lanthanides. Similar to thiocyanate, the multidentate DCA$^-$ ligand has the ability to adopt various coordinating modes from terminal binding (a) to bridging (b−d) involving one, two, or all three N positions (Scheme 1). At the same time, it has a bent shape

Scheme 1. Possible Coordinating Modes of the DCA$^-$ Ligand^a
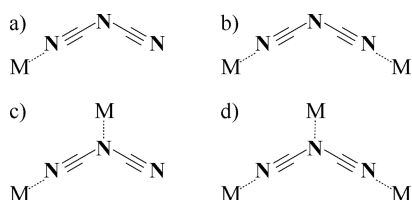
^{a}Structure c has not yet been reported for any lanthanide.

and a longer chain. However, to our knowledge, lanthanide-DCA$^-$ salts[32,33] (or actinide-DCA$^-$ salts)[34] are still rare. This suggests that new methodologies are needed to easily prepare and isolate lanthanide-DCA$^-$ salts.

To begin our exploration of, first, what factors could lead to any coordination of DCA$^-$ to lanthanides and, second, whether such salts could be designed to be ILs, we report here the synthesis and characterization of one chloride $[C_2mim]_{3n}[La-(OH_2)_4(\mu^2\text{-DCA})_4]_n[La(OH_2)_2(\mu^3\text{-DCA})_3(\mu^2\text{-DCA})_4]_{2n}(Cl)_{4n}$ (**1b**) and five isocompositional lanthanide-containing DCA$^-$-based ionic hydrates $[C_2mim][Ln(DCA)_4(H_2O)_4]$ (C_2mim = 1-ethyl-3-methylimidazolium, Ln = La (**1a**), Nd (**2**), Eu (**3**), Tb (**4**), Dy (**5**), and Yb (**6**)).

■ EXPERIMENTAL SECTION

Materials and Methods. Silver dicyanamide, Ag(DCA), was synthesized according to the literature from silver nitrate and

Na(DCA).[35] $[C_2mim][DCA]$ (≤99% purity, IoliTec, Inc., Tuscaloosa, AL), LnCl$_3$·6H$_2$O, LaCl$_3$·7H$_2$O, YbCl$_3$·6H$_2$O (99.9%, Aldrich, St. Louis, MO, USA), and $[C_2mim]Cl$ (99.9%, Merck, Kenilworth, NJ, USA) were used as received from the respective commercial sources.

Syntheses of $[C_2mim][Ln(DCA)_4(H_2O)_4]$, Ln = La (1a), Nd (2), Eu (3), Tb (4), and Dy (5). Ag(DCA) (4 mmol, 0.6956 g), LnCl$_3$·6H$_2$O (1 mmol; corresponding to 0.3587 g for Ln = Nd, 0.3664 g for Ln = Eu, 0.3734 g for Ln = Tb, 0.3770 g for Ln = Dy, and 0.3875 g for Ln = Yb), LaCl$_3$·7H$_2$O (0.3715 g), $[C_2mim]Cl$ (1 mmol, 0.1466 g), and 10 mL of DI water were mixed and stirred in a small vial (40 mL, covered with aluminum foil). A white precipitate formed immediately, and the mixtures were stirred for 2 days at room temperature. The precipitate was then filtered out and the clear solution allowed to stand in open air for water evaporation. White brick crystals formed with high yields and good qualities in 2 weeks. All attempts to obtain crystalline anhydrous complexes either by moderate heating under dynamic vacuum (100 °C) or by using various organic solvents failed. Moreover, a small water excess was found to be important for crystallization. Thermal analyses indicate that by heating to 170 °C amorphous $[C_2mim][Ln(DCA)_4]$ may form.

Synthesis of $[C_2mim]_{3n}[La(OH_2)_4(\mu^2\text{-DCA})_4]_n[La(OH_2)_2(\mu^3\text{-DCA})_3(\mu^2\text{-DCA})_4]_{2n}(Cl)_{4n}$ (1b) and $[C_2mim][Ln(DCA)_4(H_2O)_4]$, Ln = Nd (2) and Yb (6). Solid lanthanide salts, LnCl$_3$·xH$_2$O (1 mmol; LaCl$_3$·7H$_2$O, 0.3714 g; NdCl$_3$·6H$_2$O, 0.3587 g; or YbCl$_3$·6H$_2$O, 0.3875 g), and liquid $[C_2mim][DCA]$ (2 mmol, 0.3544 g) were mixed into empty borosilicate glass culture tubes (20 mL) at room temperature and slowly homogenized by hand grinding with a glass stirring rod. The obtained mixtures were placed in a heated sand bath at 40 °C for 2 days. Colorless block-shaped crystals appeared in the reaction vessels which were then allowed to cool to room temperature. Single crystals of the complexes were isolated directly from the reaction mixtures for SCXRD characterization. Additional complexation reaction attempts at different ratios were attempted (SI, Table S2) and found to be sticky solids or highly viscous liquids.

Elemental Analysis. Elemental analyses were performed on a Vario EL III elemental analyzer (Elementar Analysensysteme, Hanau, Germany).

Thermal Analysis. Phase transition temperatures were determined on a differential scanning calorimeter DSC 240 F1 (NETZSCH, Selb, Germany). Measurements were carried out at a heating rate of 5 °C/min in sealed aluminum pans with an Ar flow rate of 20 mL/min. The reference sample was an empty Al container.

Thermogravimetric analyses were carried out on a TGA-50 (Shimadzu, Kyoto, Japan) thermogravimetric analyzer at a heating rate of 10 °C min^{-1} using dry N$_2$ as the purging gas (10 mL min^{-1}).

Vibrational Spectroscopy. IR spectra were recorded on a Bruker Alpha-P FT-IR spectrometer (Bruker AXS, Karlsruhe, Germany) in the range 4000−400 cm^{-1}.

Photoluminescence Spectroscopy. Excitation and emission spectra were recorded at two different temperatures (77 and 298 K) using a Fluorolog 3 (Jobin Yvon Gmbh, München, Germany) with a Xe lamp as the excitation source and a photomultiplier tube for detection. Electronic transitions were assigned according to the energy level diagrams of trivalent rare earth ions.[36,37] The solid-state UV−vis absorption spectra were recorded on a U-3900 spectrophotometer (HITACHI, Chiyoda, Japan).

Powder X-ray Diffraction. The powder patterns of **3** and **4** were obtained with a G670 Guinier camera (Huber, Rimsting, Germany) with Mo Kα radiation. The sample was sealed in a Lindemann capillary (diameter 0.5 mm) and measured at room temperature. The powder diffraction data of **5** were recorded on a STADI P Debye−Scherrer−Geometrie powder diffractometer (STOE, Darmstadt, Germany) with Cu Kα_1 radiation (see SI).

Single Crystal X-ray Structure Determinations. Suitable crystals of **3**−**5** were selected, mounted in glass capillaries, and checked for their quality on a Stoe IPDS I single crystal X-ray diffractometer (Stoe, Darmstadt, Germany). A complete data set was measured at 100 K. Data reduction was carried out with the program package X-red,[38] and numerical absorption corrections were carried out with the program X-Shape.[39] Single crystals of **1b**, **2**, **6**, and **7**

Scheme 2. Reaction Conditions Leading to the Synthesis of 1−6

1a. $LnCl_3 \cdot nH_2O + 4Ag(DCA) + \left(\begin{array}{c} N \diagdown N \diagdown \end{array}\right) Cl \xrightarrow[H_2O]{RT} [C_2mim][Ln(DCA)_4(H_2O)_4]$
(Ln = La (**1a**), Nd (**2**), Eu (**3**), Tb (**4**), Dy (**5**))

1b. $LnCl_3 \cdot nH_2O + 4Ag(DCA) + \left(\begin{array}{c} N \diagdown N \diagdown \end{array}\right) Cl \xrightarrow[CH_3CN \text{ or } C_2H_5OH]{RT}$ **wax-like solid**

2. $LnCl_3 \cdot nH_2O + 2\left(\begin{array}{c} N \diagdown N \diagdown \end{array}\right) [DCA] \xrightarrow{40\ ^\circ C} [C_2mim][Ln(DCA)_4(H_2O)_4]$ (Ln = Nd (**2**), Yb (**6**))

$[C_2mim]_{3n}[La(OH_2)_4(\mu^2\text{-}DCA)_4]_n[La(OH_2)_2(\mu^3\text{-}DCA)_3(\mu^2\text{-}DCA)_4]_{2n}(Cl)_{4n}$ (**1b**)

were investigated using a Bruker SMART APEX2 diffractometer and those of **1a** by using a Bruker Venture diffractometer (Bruker, Madison, WI, USA).

Crystal structure solution by direct methods using SHELXT[40] yielded the space group and a majority of the atom positions. Subsequent difference Fourier analyses and least-squares refinement with SHELXL[41] allowed for the proper assignment of the atomic positions and interpretation of the disorder. In the final step of the crystal structure refinements, hydrogen atoms were added and treated with the riding atom model. The hydrogen atoms on the water molecules were located from the difference Fourier maps where possible, and their isotropic displacement factors were chosen as 1.2 times the preceding oxygen atoms.

All crystals observed in **2−5** were racemic twins yielding a Flack parameter of 0.5(1) and additional problems with the refinements of the light atom positions. A significant degree of positional/rotational disorder was observed for the DCA⁻ ligands preventing proper analysis of the C−N distances and intermolecular interactions in these compounds. Moreover, this disorder cannot be properly refined with simplified models involving a limited number of split positions and cannot be explained only by a large degree of freedom of the DCA⁻ "tails" since their connectivity is identical in all compounds except **1b**. This disorder has been modeled in reaction 1a (Scheme 2) since it was not affected by racemic twinning and could be described with the help of a split model where the DCA⁻ unit has a choice of coordination. The C₂mim⁺ cations are as a rule ordered due to strong hydrogen bonding interactions within the formed anionic framework, though high symmetry in **1a** or the charge balance requirement in **1b** led to positional and occupational disorders, respectively. Due to the high degree of positional disorder in **1a**, cations located in the cavities could not be refined, and the SQUEEZE procedure[42] was applied to account for residual electron density in the cavities, while in **1b** the minor cation disorder was modeled.

■ RESULTS AND DISCUSSION

Synthetic Methods. To overcome the weak binding of the weakly basic DCA⁻ anions to lanthanide ions, reactions of lanthanide chlorides with AgDCA were conducted in water to force coordination by forming insoluble AgCl (Scheme 2, reaction 1a). The AgDCA was added in excess to drive the complete removal of Cl⁻ and to provide an excess of DCA⁻ creating a coordination−dissociation equilibrium allowing the formation of higher coordination number compounds. Attempts to synthesize the ternary anhydrous ionic DCA⁻-based lanthanide compounds by heating under dynamic vacuum or by replacing water with organic solvents (acetonitrile or ethanol, reaction 1b) as the reaction medium failed, which only resulted in the formation of amorphous solids with waxlike consistency. Trace amounts of water are necessary to facilitate the crystal growth.

An alternative, all IL strategy was also developed on the basis of our recent work using ILs to obtain anhydrous actinide salts.[34] We hypothesized that [C₂mim][DCA] would be an ideal IL to force the coordination DCA⁻ owing to the high concentration of essentially uncoordinated DCA⁻ donor ions in the reaction. In this reaction method (Scheme 2, reaction 2), direct mixing of lanthanide halide hydrates with the IL [C₂mim][DCA] was found to produce the same compounds, except for Ln = La where its larger size allows higher coordination numbers (including more DCA⁻ in the coordination sphere) and an extra noncoordinating Cl⁻ anion was retained in the crystal structure for charge balance. Thus, in spite of the weakly coordinating nature of the soft DCA⁻ anions, they were able to substitute Cl⁻ in the coordination sphere of the lanthanides leading to isolation of the identical products, though, in contrast to actinides, water remained in the coordination sphere. The less controlled nature of this reaction methodology, however, while simple, does have its drawbacks. These reactions may also lead to crystalline byproducts such as cocrystals of the desired products and ILs.

Crystal Structures. *[C₂mim][Ln(DCA)₄(H₂O)₄] Ln = Nd (2), Eu (3), Tb (4), and Dy (5).* The isostructural series **2−5** illustrates the driving force for crystallization but also the difficulties in ever being able to obtain well-resolved crystal structures. These compounds all crystallize in the acentric monoclinic space group $P2_1$ with two formula units in the unit cell (see Table 1) and are isostructural. The eight-coordinate $[Ln(DCA)_4(H_2O)_4]^-$ anions observed in **2−5** are also found in **1a, 6,** and one of the unique La³⁺ ions in **1b**. In these anions, the Ln³⁺ ions coordinate four cyano nitrogen atoms of four terminal DCA⁻ ligands (bonding mode Scheme 1a) and four oxygen atoms of water molecules in the shape of a square antiprism (Figure 1a). The $[Ln(DCA)_4(H_2O)_4]^-$ anions serve as nodes, with the noncoordinated N atoms accepting hydrogen bonds from neighboring coordinated water molecules forming a 3D metal organic framework (MOF; Figure 1b). As a result of the size and flexibility of the framework, the central and some terminal N positions are mostly disordered since they have no set strong hydrogen bond donor to accept from. The cations in **2−5** then simply fit in the cavities optimizing their positions with weaker intermolecular interactions. Due to the nature of these structures, a more detailed and accurate analysis of these interactions will be provided on the basis of more ordered representatives with La (**1a**) and Yb (**6**) exhibiting identical motifs, but which are not isostructural.

[C₂mim][Yb(DCA)₄(H₂O)₄] (6). The smallest lanthanide studied crystallographically, Yb³⁺ (**6**), crystallizes with the same formula and general motif as **2−5**, but it is not isostructural. Compound **6** crystallizes in the centrosymmetric monoclinic space group $P2_1/c$ and represents a superstructural,

Table 1. Crystal Parameters of Compounds 1–7

	1a	1b	2	3	4	5	6	7
formula	$C_{14}H_{19}LaN_{14}O_4$	$C_{34}H_{49}La_3N_{30}O_8Cl_{14}$	$C_{14}H_{19}NdN_{14}O_4$	$C_{14}H_{19}EuN_{14}O_4$	$C_{14}H_{19}TbN_{14}O_4$	$C_{14}H_{19}DyN_{14}O_4$	$C_{14}H_{19}YbN_{14}O_4$	$C_7N_5H_9$
M	586.30	1564.56	591.67	599.39	606.35	609.93	620.47	163.19
SG	$Fddd$	$C2/c$	$P2_1$	$P2_1$	$P2_1$	$P2_1$	$P2_1/c$	$P\bar{1}$
temp, K	293	100	100	293	293	293	100	100
a, Å	9.369(5)	38.066(5)	8.6061(4)	8.521(2)	8.487(2)	8.472(2)	17.6275(12)	6.9932(4)
b, Å	21.58(1)	7.7763(8)	15.6390(8)	15.369(3)	15.343(3)	15.295(3)	15.2739(10)	8.2833(5)
c, Å	24.39(1)	23.418(3)	9.4949(4)	9.443(2)	9.408(2)	9.384(2)	16.8379(12)	8.8123(5)
α, deg								100.340(3)
β, deg		121.267(5)	110.732(3)	111.36(3)	111.08(3)	111.07(3)	95.753(2)	105.363(3)
γ, deg								113.120(3)
V, Å^3	4932(5)	5925(1)	1195.2(1)	1151.7(4)	1143.0(4)	1134.6(4)	4510.6(5)	428.94(4)
Z	8	4	2	2	2	2	8	2
D_{calc}, g cm^{-3}	1.579	1.754	1.644	1.729	1.762	1.785	1.827	1.264
μ, mm^{-1}	1.762	2.375	2.222	2.775	3.146	3.345	4.199	0.086

more ordered variant of **2–5**. The centrosymmetric model and, most important, the smaller size of Yb^{3+} led to resolution of most of the disorder problems observed in **2–5**. The overall formula and the structure of the $[Yb(DCA)_4(H_2O)_4]^-$ anion are essentially the same as those found for **2–5**; however, the packing of the anions in the crystal structure differs to a minor extent (Figure 2), which, along with the smallest size of the Yb^{3+}, apparently has a significant influence on the degree of positional disorder. The Ln positions in **2–5** form zigzag chains along the *b*-axis and order linearly along the two other directions, while those in **6** form zigzag chains along two directions (*a* and *b*) and order linearly along the *c*-direction. The tunnels observed in **2–5** are also present here, which can be visualized from a somewhat nonstandard direction approximating (301).

The complex packing observed in **6** maximizes interanionic hydrogen bonding between the DCA$^-$ and H$_2$O ligands, avoiding direct contacts between H$_2$O from different anions. The hydrogen bond network in **6** is extended and includes all N atoms from the terminal CN groups, as well as some bridging N atoms. Each water molecule binds to two nitrogen atoms from two different neighboring anions. This connectivity differs slightly from those of **1a** and **2–5** with their different degrees of involvement of nitrogen atoms in the hydrogen bonding and consequently higher degrees of their positional disorder almost directly correlating with hydrogen bonding patterns.

Another type of secondary bonding in the crystal structure of **6** includes lp–π interactions (lp = lone pair) between mostly the bridging N atoms from the DCA$^-$ ligands and the imidazole rings (d_{Cg-N} = 3.180(5)–3.324(5) Å). These interactions in fact involve all N atoms not participating in bonding with Yb or hydrogen bonding with H$_2$O ligands. These interactions though cannot be considered as somehow important for the framework formation but rather help cations to simply fit in the cavities optimizing their positions.

[C$_2$mim][La(DCA)$_4$(H$_2$O)$_4$] (1a). Compound **1a** crystallizes in the orthorhombic space group *Fddd* and is another superstructural variant of **2–5**. The *bc* diagonal of **1a** is approximately equivalent to 4 unit cell parameters *a* of **2–5** that can be explained by identical building units. The anion $[La(DCA)_4(H_2O)_4]^-$ in **1a**, as well as its connectivity, is practically identical to those of **2–5** resulting in an analogous 3D MOF (Figure 3) with encapsulated C$_2$mim$^+$ cations as discussed above. Due to the high symmetry and high degree of positional disorder of the DCA$^-$ ligands, the C$_2$mim$^+$ cations could not even be observed from the difference Fourier maps. The high degree of positional disorder of the central N atom also correlates well with the larger size of the La^{3+} ion compared to, e.g., Yb^{3+} where such disorder was not observed at all.

[C$_2$mim]$_{3n}$[La(OH$_2$)$_4$(μ^2-DCA)$_4$]$_n$[La(OH$_2$)$_2$(μ^3-DCA)$_3$(μ^2-DCA)$_4$]$_{2n}$(Cl)$_{4n}$ (1b). Compound **1b** was isolated by direct dissolution of LaCl$_3$·7H$_2$O in [C$_2$mim][DCA], and the presence of Cl$^-$ clearly disrupted formation of **1a** although there are similarities as discussed below. It is somewhat remarkable that, even though in this synthetic route Cl$^-$ remained in solution and could be competitive with DCA$^-$, it did not directly coordinate La^{3+}. Consequently, **1b** which crystallized in *C2/c*, might be viewed as a product of partial chloride substitution or a cocrystal or double salt.

The larger size of La^{3+} in **1b** is apparent in the competition for 8-coordination and 9-coordination and the formation of a
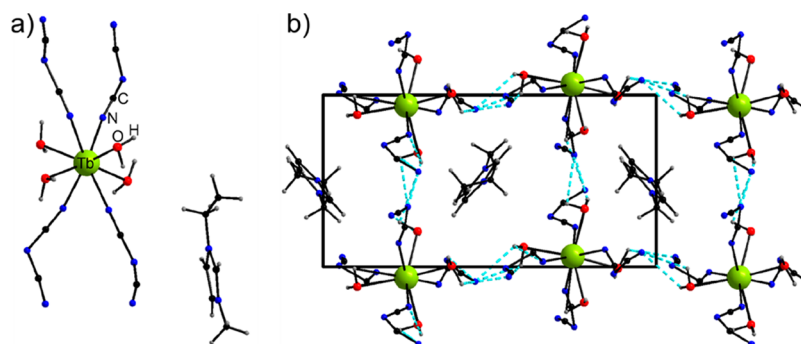
Figure 1. Asymmetric unit (a) and 3D structure of **2–5** represented with Ln = Tb (**4**) viewed down the *c*-axis (b). The O−H···N bonds are presented as dashed lines.
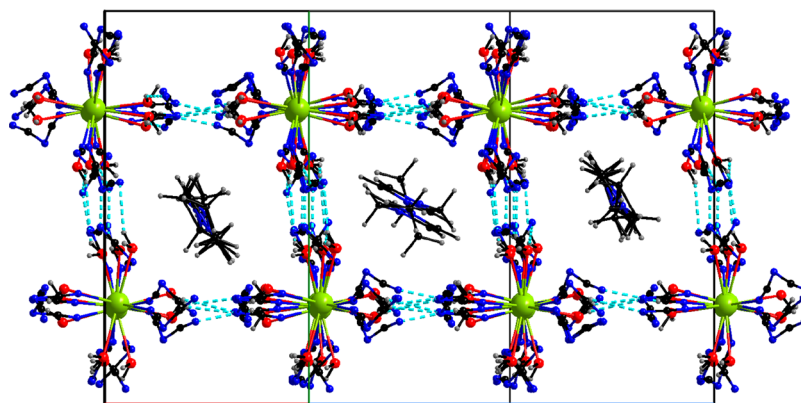
Figure 2. (a) Projection of the crystal structure of **6** on (301). The O−H···N bonds are presented as dashed lines. Crystallographic axes are color coded: *a*, red; *b*, green; *c*, blue.
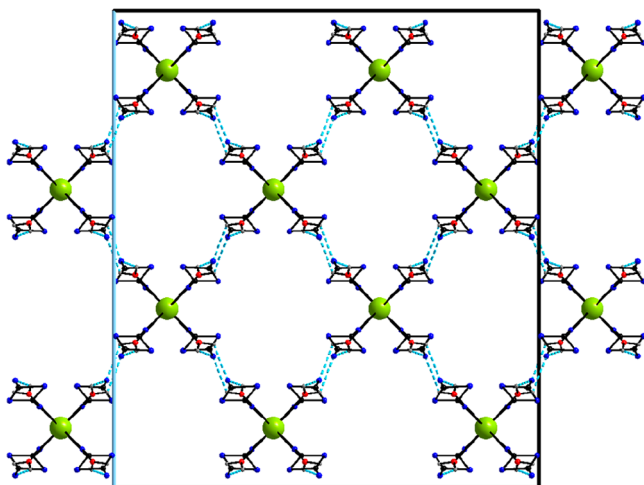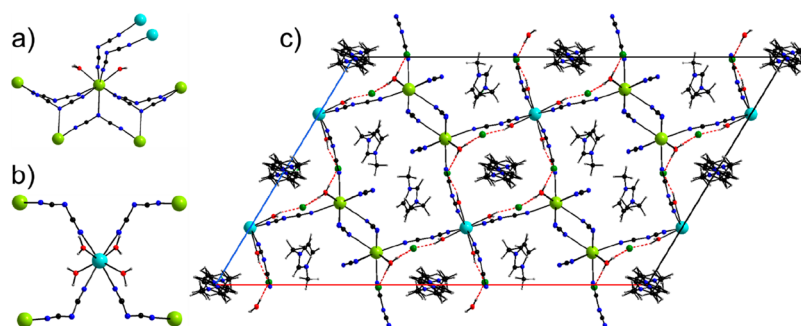

Figure 3. Projection of the crystal structure of compound **1a** along the *a*-axis. The cations are not shown and were neither found nor refined as discussed above.

more traditional MOF supported by bridging ligands rather than by hydrogen bonding. One of the La³⁺ positions (La2) has all of the common features found for the anions in **2–6** including tetrahedral coordination by 4 terminal N atoms of the DCA⁻ groups and 4 H_2O ligands. The other one (La1) is coordinated by 7 DCA⁻ anions and only 2 H_2O molecules (Figure 4a) and brings something unique to the system: coordination of the lanthanide to the bridging N position of a DCA⁻ anion (resulting in the bonding mode in Scheme 1d).

This type of Ln-DCA⁻ connectivity has thus far only been observed in *anhydrous* lanthanide-DCA⁻ salts,[43] and the ability of DCA⁻ to compete with the strongly coordinating O-donor is at least unusual but of practical interest in the substitution of the latter in their coordination compounds, e.g., hydrates. The degree of participation of the DCA⁻ central N atom shows a direct correlation with the degree of H_2O substitution confirming our hypothesis and deserves further studies.

All La positions are interconnected with the DCA⁻ ligands in two different modes. The 8-coordinated La atoms bind to four 9-coordinated ones using only terminating N atoms, while 9-coordinated La centers bind to two 8-coordinated atoms and additionally have double connections to two 9-coordinated atoms along the *b*-direction, realized though the involvement of *all three N atoms from the DCA⁻ ligands*. All four μ^2 bridges around La2 go solely to La1 positions, while connectivity around La1 is much more complicated. There are two μ^2 bridges to La2, two μ^2 bridges to neighboring La1, and two additional μ^3 bridges to the same two La1 and two new La1. The latter two are reinforced by an additional μ^3 bridge with the central N connectivity to the described position (Figure 4a,b).

The overall connectivity results in a 3D coordination net with channels along the *b*-direction encapsulating the organic cations. These channels in turn have two different shapes and form checkered motifs along the *ac* diagonal (Figure 4c). One of the channels has a square appearance with four vertices, while another one is a truncated rectangle with six vertices as the result of double nodes formed by La1 positions.

Figure 4. Coordination and connectivity around (a) La(1) and (b) La(2) in **1b**, and (c) projection of its crystal structure along the *b*-axis: 8-coordinated La are blue, and 9-coordinated are green. Crystallographic axes are color coded *a*, red; *c*, blue.

Table 2. Selected Bond Lengths (Å) in 1−6 and Related Dicyanamide Salts

	Ln−O(W)	Ln−N(t)^a	Ln−N(m)^a	DCA⁻ mode^b
Sr[N(CN)$_2$]$_2$[43]		2.622(5)−2.738(4)	2.771(4)	D
Ba[N(CN)$_2$]$_2$[43]		2.827(1)−2.923(2)	2.935(2)−2.993(2)	D
La[N(CN)$_2$]$_3$^{c,32}		2.62(2)−2.68(2)	2.38(4)−2.82(2)	D
Eu[N(CN)$_2$]$_3$^{c,32}		2.38(4)−2.50(2)	2.72(3)−2.88(2)	D
Eu[N(CN)$_2$]$_3$·2H$_2$O[33]	2.37(4)−2.41(6)	2.49(1)−2.62(2)		B
1a	2.460(5)	2.581(5)		A
1b	2.475(4)−2.502(4)	2.594(6)−2.675(8)	2.867(5)	B + D
2	2.35(2)−2.44(3)	2.47(3)−2.56(3)		A
3	2.32(1)−2.41(1)	2.48(1)−2.51(1)		A
4	2.27(1)−2.41(1)	2.43(1)−2.48(1)		A
5	2.27(1)−2.39(1)	2.41(1)−2.49(4)		A
6	2.259(4)−2.314(3)	2.405(4)−2.431(3)		A

^{a}t, terminal; m, middle. ^{b}Please refer to Scheme 1. ^{c}Geometry of the DCA⁻ ligand significantly differs from the usual geometry.

The La−O$_w$ (2.460(5) Å) and La−N (2.581(5) Å) distances in **1a** are slightly shorter than in La(DCA)$_3$ and in **1b** (Table 2). The La−N bonds in **1a** to the bridging N positions of the DCA⁻ ligands (Ln−N(m)) are ∼10% longer (Table 2) than those in the terminal coordination mode (Ln−N(t)), though the La−La distances in those zigzag chains are considerably shorter (6.6468(8) Å, Figure 4b, green−green) compared to those in the squares (8.811(1) Å, Figure 4b, green−blue). A comparable elongation of the bridging N distances to the metal atoms has also been observed in the alkaline-earth DCA⁻ salts.[32,43]

The secondary bonding picture in the crystal packing of **1b** is also completely different from those observed in **2−6**. It is dominated by an extended OH···Cl hydrogen bonding network complemented by weaker CH···Cl and CH···N hydrogen bonds. No π−π, CH···π, or lp−π bonds have been observed in this structure. Each Cl position coordinates three water molecules and two organic cations. The C$_2$mim⁺ cations in the square channels are positionally disordered as a consequence of the high symmetry of the latter.

[C₁mim][DCA]. We have found the environment around DCA⁻ to be qualitatively informative of its charge distribution[34] and thus sought to compare changes in polarity of the C≡N and C−N bonds with and without the lanthanide ions. In this context, we crystallized and analyzed the packing of [C₁mim][DCA] obtained in our previous work,[44] since the [C₂mim][DCA] salt used for the reactions studied here could not be crystallized.[45] Extensive hydrogen bonding between the terminating DCA⁻ N positions and practically all H positions is present in its crystal packing (Figure 5). Reasonably, the N position bound to one C₁mim⁺ shows stronger H bonding
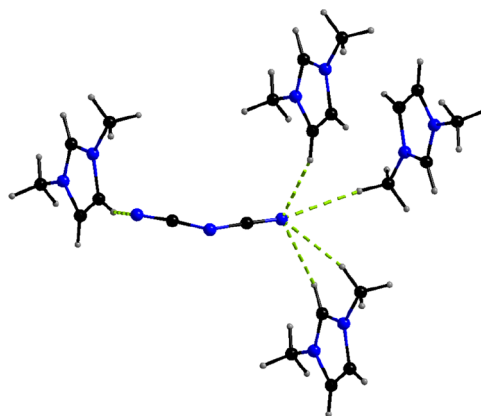

Figure 5. Packing environment around the DCA⁻ in the crystal structure of [C₁mim][DCA].

($d_{CH···N}$ = 2.39(2) Å) than the one bound to three ($d_{CH···N}$ = 2.53(2)−2.64(2) Å). Additionally, the cations strongly π−π stack ($d_{Cg−Cg}$ = 3.567−3.760(1) Å).

Given the extensive disorder in **2−5**, we can realistically only compare the C≡N and C−N bonds to those in **1a**, **1b**, and **6**. In [C₁mim][DCA], the C≡N and C−N bonds are 1.158(2) and 1.306−1.310(2) Å, respectively. The corresponding distances in **1b** are 1.135(7)−1.161(8) and 1.301(9)−1.328(8) Å, and in **6** they are 1.143−1.160(6) and 1.279−1.315(7) Å. Overall, there appears to be little influence of metal coordination on the C···N bonding. This is consistent with [DCA]⁻ ions, for which the negative charge resides primarily on the nitrile groups,[46] interacting electrostatically
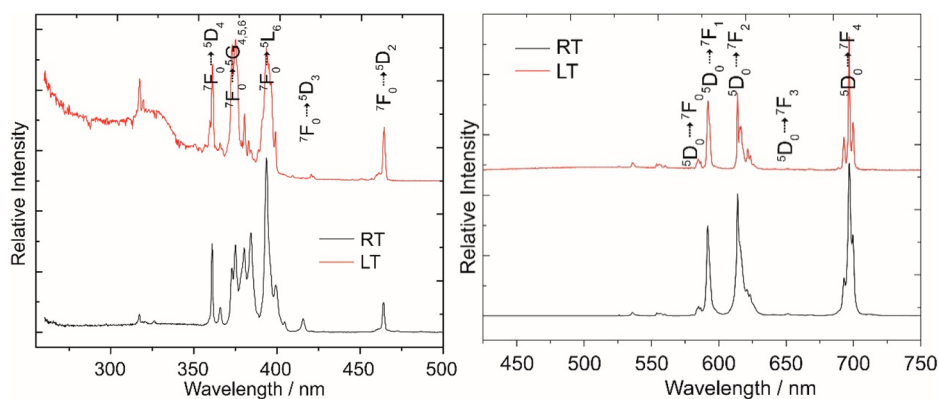
Figure 6. Excitation (left, λ_{em} = 612 nm) and emission (right, λ_{ex} = 394 nm) spectra of **3**.
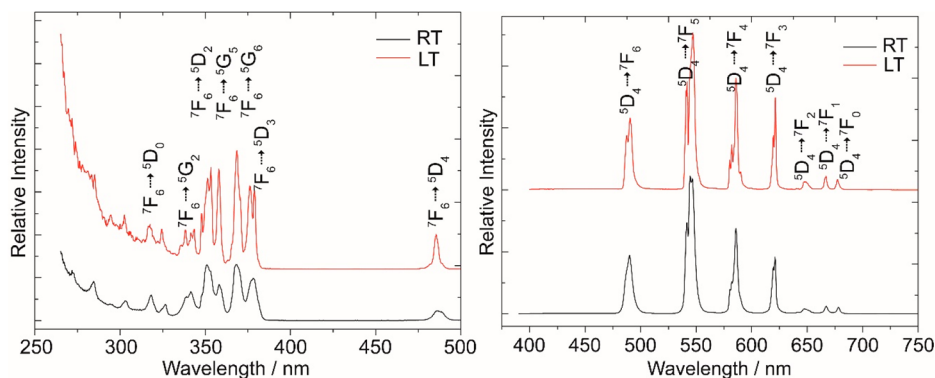
Figure 7. Excitation (left, λ_{ex} = 547 nm) and emission (right, λ_{ex} = 368 nm) spectra of **4**.

with the metal ions in a manner which does not result in significant electron transfer.

Photophysical Investigations. Isolation of this series of compounds allowed us to further characterize selected members of the series. The excitation and emission spectra of compounds **3–5** which contain lanthanide ions that are able to show visible light emission (Eu^{3+}, Tb^{3+}, and Dy^{3+}) were recorded at both room (RT) and liquid nitrogen (LT) temperatures. The respective spectra all show the corresponding characteristic f–f transitions.

The excitation spectrum for **3** (Figure 6) was monitored at 612 nm (the $^5D_0 \rightarrow {}^7F_2$ emission of Eu^{3+}). At RT, the excitation spectrum is mainly dominated by a series of narrow and intense lines: 361, 366 ($^7F_0 \rightarrow {}^5D_4$), 373, 375 ($^7F_{0/1} \rightarrow {}^5G_J$), 380.25, 384.25 ($^7F_{0/1} \rightarrow {}^5L_7, {}^5G_J$), 393.75, 399.5 ($^7F_0 \rightarrow {}^5L_6$), 415.75 ($^7F_0 \rightarrow {}^5D_3$), and 464 ($^7F_0 \rightarrow {}^5D_2$), which is different from those of $Eu(DCA)_3 \cdot 2H_2O$[33] and $Eu(DCA)_3$,[32] where the excitation spectra are all dominated by a broad band in the range 260–420 nm, probably due to effective energy transfer from the ligand to the europium(III) center. At LT, the discrete f–f transitions become more intense and sharper, but the most remarkable change was observed in the broad band between 250 and 350 nm, corresponding to the $\pi–\pi^*$ transitions of the DCA^- ligand.[33] It increases in intensity at LT, indicating the ability of the DCA^- ligand to transfer energy to Eu^{3+}.

Complex **3** also exhibits the characteristic intense transitions of the Eu^{3+} ion upon excitation at 394 nm. At RT the transitions from the excited $^5D_0$ state to the different J levels of the lower ^7F state were observed in the emission spectrum at 579.5 ($^5D_0 \rightarrow {}^7F_0$), 583.75, 585, 586.25, and 591.75 ($^5D_0 \rightarrow$

$^7F_1$), 614, 621, 623.25 ($^5D_0 \rightarrow {}^7F_2$), 651.25 ($^5D_0 \rightarrow {}^7F_3$), and 693, 697, 699.5 nm ($^5D_0 \rightarrow {}^7F_4$) (Figure 6). The spectrum is mainly dominated by the hypersensitive transitions $^5D_0 \rightarrow {}^7F_4$ and $^5D_0 \rightarrow {}^7F_2$ indicating a low point symmetry for Eu^{3+}. Moreover, the presence of only one sharp peak in the region of the $^5D_0 \rightarrow {}^7F_0$ transition at 579.5 nm suggests the existence of a single chemical environment around the Eu^{3+} ion, which is in good agreement with the X-ray crystal structure of **3**. The position and shape of the emission lines are similar to those of $Eu(DCA)_3 \cdot 2H_2O$ and $Eu(DCA)_3$, but the relative intensities are different due to their different coordination environment symmetries.[33]

Although the emission was mainly from the $^5D_0$ level, the transitions from the higher energy $^5D_1$ level to the $^7F_{0-1}$ state (526, 535.75, 554, 557, and 559.75 nm) can also be observed. Lowering the temperature leads to typical line narrowing and well-resolved $2J + 1$ Stark components splitting multiplets due to the removal of the vibronic contributions, as well as to the change of the relative intensities of the respective transitions and therefore a significant change of the emission color (Figure 9). The intensity ratio of the first electric and the magnetic dipole transition gives valuable information on the coordination environment of Eu^{3+} and, therefore, is usually taken as the asymmetry parameter.[47] At RT, the $I(^5D_0 \rightarrow {}^7F_2)/I(^5D_0 \rightarrow {}^7F_1)$ ratio of **3** is about 1.35, but it decreases to about 1.03 at LT (77 K) indicating a higher symmetric environment of the Eu^{3+} center. The decay time of **3** was found to be approximately 0.22 ms at both 77 and 298 K, and the decay curve can be fitted with a single exponential function supporting the presence of only one Eu^{3+} species.
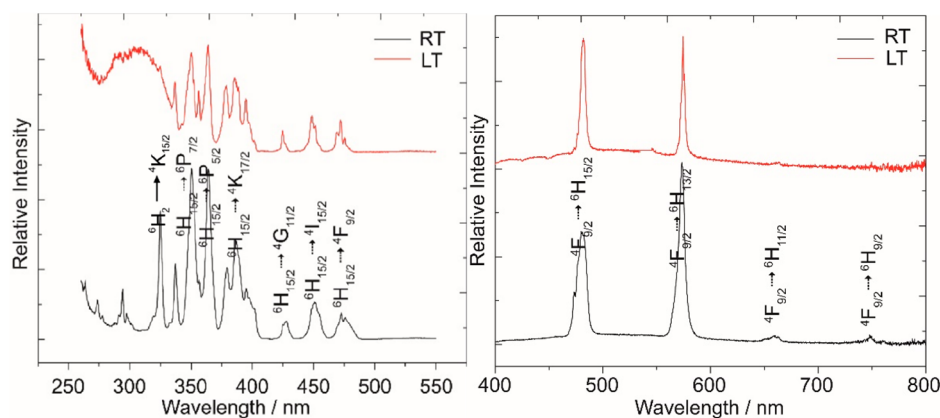
**Figure 8.** Excitation (left, λ_{em} = 574 nm) and emission (right, λ_{ex} = 368 nm) spectra of **5**.

The steady-state excitation and emission spectra of **4** in the solid state at both RT and LT are shown in Figure 7. The excitation spectrum monitored around the peak of the intense $^5D_4 \rightarrow {}^7F_5$ transition (547 nm) of the Tb^{3+} ion exhibits several narrow bands arising from 4f–4f intraconfigurational transitions from the ground-state $^7F_6$ level to the different excited states of Tb^{3+}, i.e., 318.25 ($^5D_0$), 339, 341.5 ($^5G_2$), 350.75 ($^5D_2$), 358 ($^5G_5$), 368 ($^5G_6$), 378 ($^5D_3$), and 485.5 nm ($^5D_4$).

Five sets of sharp lines assigned to transitions from the $^5D_4$ excited state to the different J levels of the ground term ^7F (^7F_J, J = 6–0) are found in the emission spectrum at about 489.75 ($^5D_4 \rightarrow {}^7F_6$), 541.75, 544.5, 546.5 ($^5D_4 \rightarrow {}^7F_5$), 580.5, 582, 585.75 ($^5D_4 \rightarrow {}^7F_4$), 619.5, 621 ($^5D_4 \rightarrow {}^7F_3$), 641.75, 647 ($^5D_4 \rightarrow {}^7F_2$), 667.25 ($^5D_4 \rightarrow {}^7F_1$), 678.25 ($^5D_4 \rightarrow {}^7F_0$). The most intense emission is centered at 545 nm and corresponds to the transition $^5D_4 \rightarrow {}^7F_5$. The change of temperature has a very tiny effect on the position of emission; only slight band narrowing and splitting were observed. The emission spectra are similar to those of $Tb[N(CN)_2]_3 \cdot 2H_2O$ and $Tb[N(CN)_2]_3$, while the relative intensities are different indicating different local symmetries around the terbium(III) center.[33] The decay time of **4** showed minor temperature sensitivity. The Tb^{3+} ($^5D_4$) lifetime ($\lambda_{ex,em}$ = 368, 547 nm) increased from 0.60 to 0.71 ms at LT.

The photoluminescence of the Dy^{3+} compound **5** was studied at RT and LT as well (Figure 8). The excitation spectrum of **5** shows the f–f transitions characteristic for Dy^{3+} at about 350 nm. Compound **5** exhibits two apparent emission bands under the excitation of 368 nm with the maximum emission wavelengths of 480, 573.5 nm at RT and 482, 574.5 nm at LT, respectively, which can be ascribed to the characteristic $^4F_{9/2} \rightarrow {}^6H_{15/2}$ and $^4F_{9/2} \rightarrow {}^6H_{13/2}$ transitions of Dy^{3+}. The weak intense bands at 660 and 747.75 nm correspond to the $^4F_{9/2} \rightarrow {}^6H_{11/2}$ and $^4F_{9/2} \rightarrow {}^6H_{9/2}$ transitions.

Similar to the electric dipole transition of $^5D_0 \rightarrow {}^7F_2$ for Eu^{3+}, the $^4F_{9/2} \rightarrow {}^6H_{13/2}$ transition of Dy^{3+} is a hypersensitive transition (ΔL = 2, ΔJ = 2) and is strongly influenced by the local environment of the trivalent lanthanide cation.[48] Its intensity strongly determines the visible appearance of the luminescent dysprosium compound; depending on the intensity ratios of the $^4F_{9/2} \rightarrow {}^6H_{15/2}$ and $^4F_{9/2} \rightarrow {}^6H_{13/2}$ transitions, the emission has either a whitish or green/yellowish color (Figure 9).[48] The $^4F_{9/2} \rightarrow {}^6H_{13/2}$ transition at 573.5 nm is the most intense for **5** in agreement with the yellowish luminescence of the sample.
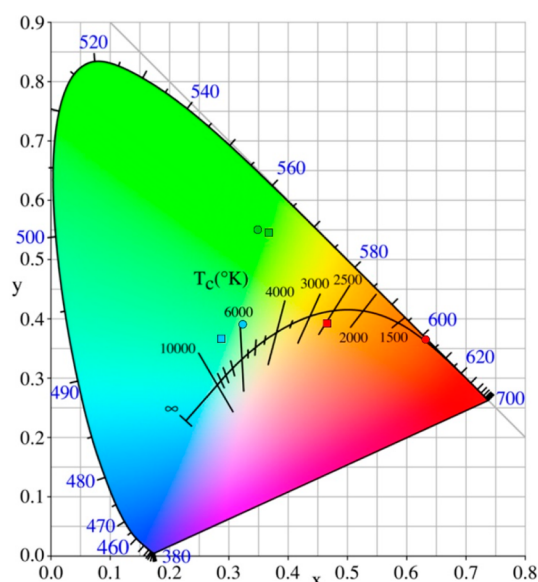
Figure 9. CIE 1931 chromaticity diagram for **3**–**5** [red, **3**; green, **4**; blue, **5**; circle, at RT; square, at LT (77 K)]. The respective (x, y) coordinates can be found in SI, Table S1.

The Dy^{3+} ($^4F_{9/2}$) decay can be well-fitted with a monoexponential function to yield a decay time of 11.9 μs, indicating that only one Dy^{3+} species is present, as is obvious from its crystal structure. This value is comparable to that of the series of dysprosium-based ILs $[C_6mim]_{5-x}[Dy-(SCN)_{8-x}(H_2O)_x]$ (x = 0–2)[12] but shorter than that of $Dy(Tf_2N)_3$ in $[bmpyr][Tf_2N]$[49] and DyI_3 in the IL $[C_{12}mim]-[Tf_2N]$.[50]

The CIE coordinates of compounds **3**–**5** have been calculated from the respective RT and LT emission spectra (Figure 9), which clearly indicate their emission colors in the red, green-yellow, and blue-yellow regions, respectively. It is noted that the CIE coordinates of compound **3** are comparable to those of $Eu(DCA)_3 \cdot 2H_2O$ and $Eu(DCA)_3$, while the terbium compound emits in a more yellowish region.[33]

Thermal Stability and Behavior. The thermal stabilities of compounds **3**–**5** were examined by thermogravimetric analysis (TG) in the temperature range 25–500 °C (Figure S3). Since the three complexes are isostructural, similar thermal behaviors were observed. All compounds show two significant weight losses. The initial weight loss of 10.76%

7234

(calcd 12.02%) for **3**, 11.25% (calcd 11.89%) for **4**, and 10% (calcd 11.82%) for **5** in the range 60−165 °C corresponds to the removal of the four coordinated water molecules. On closer inspection, this first weight loss appears to occur in two, hard to resolve thermal events, which could point to the intermediate formation of a coordination polymer upon dehydration. No thermal events were observed between 170 and 250 °C. The DCA⁻ ligands begin to decompose above 300 °C (earlier than the major decomposition that occurs for the hydrated lanthanide dicyanamide salts which start at 450 °C).[33] At 500 °C, the decomposition is not complete.

The thermal behaviors of compounds **3−5** were also investigated by differential scanning calorimetry (DSC), Figure 10. All compounds show similar thermal events. For
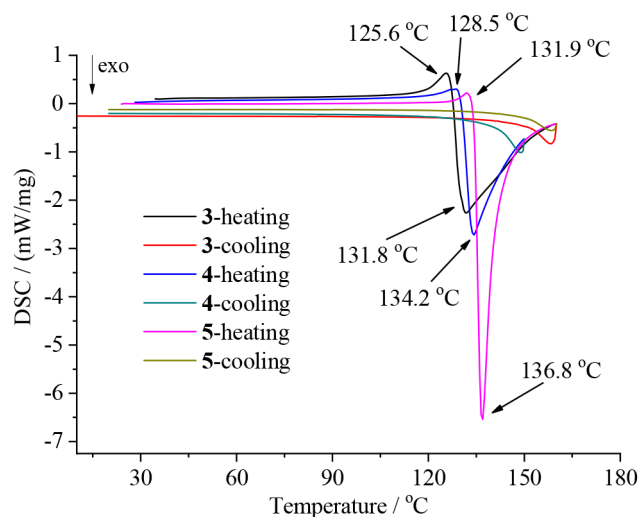
Figure 10. DSC thermograms of compounds **3−5** recorded at 5 °C/min.

compound **3**, an endothermic peak at about 125.6 °C can be observed on the first heating trace followed by a broad and strong exothermic peak. Combined with the TG result, this suggest that it starts to melt at above 120 °C, but almost at the same time it starts to lose the coordinated water molecules. For compounds **4** and **5**, the endo- and exothermic peaks are found at 128.5 and 134.2 °C for **4** and 131.9 and 136.8 °C for **5**, respectively. Obviously, their thermal behaviors are not reversible. A small increase of the melting temperature is observed in the row Eu−Tb−Dy, going in parallel with an increasing molecular weight.

Conclusions. A series of lanthanide-containing DCA⁻-based ionic compounds have been successfully synthesized by simple reaction of lanthanide chlorides hydrates with [C₂mim]Cl and Ag(DCA) generated *in situ* in the IL or by dissolution in the IL [C₂mim][DCA]. The latter has the disadvantage of leaving Cl⁻ in solution. The isolation of [C₂mim][Ln-(DCA)₄(H₂O)₄] [Ln = La (**1a**), Nd (**2**), Eu (**3**), Tb (**4**), Dy (**5**), and Yb (**6**)] using both routes led to three superstructural variants (**1a**, **2−5**, **6**) with essentially the same motif: [Ln(DCA)₄(H₂O)₄]⁻ with four terminal, end-on coordinated DCA⁻ ligands serving as nodes and the non-coordinated N atoms accepting hydrogen bonds from neighboring coordinated water molecules resulting in 3D MOFs. By comparison to the structure of the metal-free salt, [C₁mim][DCA], it is clear that coordination to the metal

centers does not seriously affect the chemical structure and bonding within the DCA⁻ ligands.

The presence of free Cl⁻ in the second synthetic route and the larger size of La³⁺ led to the isolation of [C₂mim]₃ₙ[La-(OH₂)₄(μ²-DCA)₄]ₙ[La(OH₂)₂(μ³-DCA)₃(μ²-DCA)₄]₂ₙ(Cl)₄ₙ (**1b**). This compound features two crystallographically unique La³⁺ sites, one of which is similar to that observed in the chloride-free salts and the second of which is 9-coordinate. In this structure, the formation of a two-component MOF is supported by the more traditional coordinative ligand bridging. Formally, the structure can be described as a cocrystal of La(DCA)ₙ and C₂mimCl, though with an extra noncoordinated Cl⁻ anion to compensate charge.

At above 125 °C, these compounds start to melt and release the coordinating water molecules transforming into waxlike substances. Further work and new synthetic strategies are required to examine the possibility and approach water-free crystalline products. The further heating above 300 °C leads to the final decomposition with loss of the DCA⁻ ligands. The photophysical properties of **3−5** were studied revealing characteristic f−f transitions for each lanthanide and moderate lifetimes in the millisecond to microsecond range. Among the examined complexes, the Eu one revealed the most significant change of the emission color upon cooling from red to orange/yellow.

■ ASSOCIATED CONTENT

Ⓢ Supporting Information

The Supporting Information is available free of charge at https://pubs.acs.org/doi/10.1021/acs.inorgchem.0c00667.

> Powder XRD patterns, IR spectra, additional crystallographic data and synthesis details, chemical analysis results, and CIE coordinates (PDF)

Accession Codes

CCDC 1972255−1972258 and 1976652 contain the supplementary crystallographic data for this paper. These data can be obtained free of charge via www.ccdc.cam.ac.uk/data_request/cif, or by emailing data_request@ccdc.cam.ac.uk, or by contacting The Cambridge Crystallographic Data Centre, 12 Union Road, Cambridge CB2 1EZ, UK; fax: +44 1223 336033.

■ AUTHOR INFORMATION

Corresponding Authors

> **Robin D. Rogers** − *Department of Materials and Environmental Chemistry, Stockholm University, 10691 Stockholm, Sweden; College of Arts & Sciences, The University of Alabama, Tuscaloosa, Alabama 35487, United States;* ⓘ orcid.org/0000-0001-9843-7494; Email: rdrogers@ua.edu
>
> **Anja-Verena Mudring** − *Department of Materials and Environmental Chemistry, Stockholm University, 10691 Stockholm, Sweden;* ⓘ orcid.org/0000-0002-2800-1684; Email: anja-verena.mudring@mmk.su.se

Authors

> **Si-Fu Tang** − *College of Chemistry and Pharmaceutical Sciences, Qingdao Agricultural University, Qingdao 266109, China;* ⓘ orcid.org/0000-0002-7151-9876
>
> **Volodymyr Smetana** − *Department of Materials and Environmental Chemistry, Stockholm University, 10691 Stockholm, Sweden;* ⓘ orcid.org/0000-0003-0763-1457

Manish Kumar Mishra − *College of Arts & Sciences, The University of Alabama, Tuscaloosa, Alabama 35487, United States*

Steven P. Kelley − *College of Arts & Sciences, The University of Alabama, Tuscaloosa, Alabama 35487, United States;* ⓘ orcid.org/0000-0001-6755-4495

Olivier Renier − *Department of Materials and Environmental Chemistry, Stockholm University, 10691 Stockholm, Sweden;* ⓘ orcid.org/0000-0002-1227-547X

Complete contact information is available at:
https://pubs.acs.org/10.1021/acs.inorgchem.0c00667

Notes

The authors declare no competing financial interest.

■ REFERENCES

(1) Lei, Z.; Chen, B.; Koo, Y.-M.; MacFarlane, D. R. Introduction: Ionic Liquids. *Chem. Rev.* **2017**, *117*, 6633−6635.

(2) Seddon, K. R. Ionic Liquids for Clean Technology. *J. Chem. Technol. Biotechnol.* **1997**, *68*, 351−356.

(3) Seddon, K. Room-temperature ionic liquids: neoteric solvents for clean catalysis. *Kinet. Catal.* **1995**, *37*, 693−697.

(4) Earle, M. J.; Seddon, K. R. Ionic liquids. Green solvents for the future. *Pure Appl. Chem.* **2000**, *72*, 1391−1398.

(5) Welton, T. Room-temperature ionic liquids. Solvents for synthesis and catalysis. *Chem. Rev.* **1999**, *99*, 2071−2084.

(6) Wasserscheid, P.; Keim, W. Ionic Liquids—New "Solutions" for Transition Metal Catalysis. *Angew. Chem., Int. Ed.* **2000**, *39*, 3772−3789.

(7) Picquet, M.; Tkatchenko, I.; Tommasi, I.; Wasserscheid, P.; Zimmermann, J. Ionic Liquids, 3. Synthesis and Utilisation of Protic Imidazolium Salts in Homogeneous Catalysis. *Adv. Synth. Catal.* **2003**, *345*, 959−962.

(8) Wasserscheid, P.; Welton, T. *Ionic Liquids in Synthesis*; John Wiley & Sons, 2008.

(9) Hallett, J. P.; Welton, T. Room-Temperature Ionic Liquids: Solvents for Synthesis and Catalysis. 2. *Chem. Rev.* **2011**, *111*, 3508−3576.

(10) Prodius, D.; Mudring, A.-V. Coordination Chemistry in Rare Earth Containing Ionic Liquids In *Handbook on the Physics and Chemistry of Rare Earths*; Bünzli, J.-C. G., Pecharsky, V. K., Eds.; Elsevier, 2016; Vol. *50*, pp 395−420.

(11) Mudring, A. V.; Tang, S. Ionic liquids for lanthanide and actinide chemistry. *Eur. J. Inorg. Chem.* **2010**, *2010*, 2569−2581.

(12) Mallick, B.; Balke, B.; Felser, C.; Mudring, A.-V. Dysprosium Room-Temperature Ionic Liquids with Strong Luminescence and Response to Magnetic Fields. *Angew. Chem., Int. Ed.* **2008**, *47*, 7635−7638.

(13) Tang, S.; Babai, A.; Mudring, A.-V. Europium-Based Ionic Liquids as Luminescent Soft Materials. *Angew. Chem., Int. Ed.* **2008**, *47*, 7631−7634.

(14) Tang, S.; Cybinska, J.; Mudring, A. V. Luminescent Soft Material: Two New Europium-Based Ionic Liquids. *Helv. Chim. Acta* **2009**, *92*, 2375−2386.

(15) Tang, S.-F.; Lorbeer, C.; Wang, X.; Ghosh, P.; Mudring, A.-V. Highly Luminescent Salts Containing Well-Shielded Lanthanide-Centered Complex Anions and Bulky Imidazolium Countercations. *Inorg. Chem.* **2014**, *53*, 9027−9035.

(16) Li, H.; Shao, H.; Wang, Y.; Qin, D.; Liu, B.; Zhang, W.; Yan, W. Soft material with intense photoluminescence obtained by dissolving Eu$_2$O$_3$ and organic ligand into a task-specific ionic liquid. *Chem. Commun.* **2008**, 5209−5211.

(17) Li, H.; Liu, P.; Shao, H.; Wang, Y.; Zheng, Y.; Sun, Z.; Chen, Y. Green synthesis of luminescent soft materials derived from task-specific ionic liquid for solubilizing lanthanide oxides and organic ligand. *J. Mater. Chem.* **2009**, *19*, 5533−5540.

(18) Wang, D.; Wang, H.; Li, H. Novel luminescent soft materials of terpyridine-containing ionic liquids and europium (III). *ACS Appl. Mater. Interfaces* **2013**, *5*, 6268−6275.

(19) Pereira, C. C. L.; Dias, S.; Coutinho, I.; Leal, J. P.; Branco, L. C.; Laia, C. A. T. Europium(III) Tetrakis(β-diketonate) Complex as an Ionic Liquid: A Calorimetric and Spectroscopic Study. *Inorg. Chem.* **2013**, *52*, 3755−3764.

(20) Ji, S.-P.; Tang, M.; He, L.; Tao, G.-H. Water-Free Rare-Earth-Metal Ionic Liquids/Ionic Liquid Crystals Based on Hexanitratolanthanate(III) Anion. *Chem. - Eur. J.* **2013**, *19*, 4452−4461.

(21) Babai, A.; Pitula, S.; Mudring, A.-V. Structural and Electrochemical Properties of Yb^{III} in Various Ionic Liquids. *Eur. J. Inorg. Chem.* **2010**, *2010*, 4933−4937.

(22) Prodius, D.; Mudring, A.-V. Rare earth metal-containing ionic liquids. *Coord. Chem. Rev.* **2018**, *363*, 1−16.

(23) Babai, A.; Kopiec, G.; Lackmann, A.; Mallick, B.; Pitula, S.; Tang, S.; Mudring, A.-V. Eu^{3+} as a dual probe for the determination of IL anion donor power: A combined luminescence spectroscopic and electrochemical approach. *J. Mol. Liq.* **2014**, *192*, 191−198.

(24) Tang, S.; Mudring, A.-V. Ionic Liquids as Crystallization Media: Weakly-Coordinating Anions Do Coordinate in 1_{∞}[Eu-(OTf)$_3$(CH$_3$CN)$_3$]. *Cryst. Growth Des.* **2011**, *11*, 1437−1440.

(25) Tang, S.-F.; Mudring, A.-V. The Missing Link Crystallized from the Ionic Liquid 1-Ethyl-3-methylimidazolium Tosylate: Bis-aqua-(p-toluenesulfonato-O)-europium(III)-bis-p-toluenesulfonate Dihydrate. *Cryst. Growth Des.* **2009**, *9*, 2549−2551.

(26) Nockemann, P.; Thijs, B.; Postelmans, N.; Van Hecke, K.; Van Meervelt, L.; Binnemans, K. Anionic Rare-Earth Thiocyanate Complexes as Building Blocks for Low-Melting Metal-Containing Ionic Liquids. *J. Am. Chem. Soc.* **2006**, *128*, 13658−13659.

(27) Tang, S.-F.; Mudring, A.-V. Highly Luminescent Ionic Liquids Based on Complex Lanthanide Saccharinates. *Inorg. Chem.* **2019**, *58*, 11569−11578.

(28) MacFarlane, D. R.; Golding, J.; Forsyth, S.; Forsyth, M.; Deacon, G. B. Low viscosity ionic liquids based on organic salts of the dicyanamide anion. *Chem. Commun.* **2001**, 1430−1431.

(29) Yoshida, Y.; Baba, O.; Saito, G. Ionic Liquids Based on Dicyanamide Anion: Influence of Structural Variations in Cationic Structures on Ionic Conductivity. *J. Phys. Chem. B* **2007**, *111*, 4742−4749.

(30) Boudesocque, S.; Mohamadou, A.; Dupont, L.; Martinez, A.; Déchamps, I. Use of dicyanamide ionic liquids for extraction of metal ions. *RSC Adv.* **2016**, *6*, 107894−107904.

(31) Zhang, X.; Zhang, L.-Y.; Shi, L.-X.; Chen, Z.-N. Cyclometallated iridium(III) complexes with dicyanamide or tricyanomethanide. *Inorg. Chem. Commun.* **2009**, *12*, 758−760.

(32) Jürgens, B.; Irran, E.; Schnick, W. Synthesis and characterization of the rare-earth dicyanamides Ln[N(CN)$_2$]$_3$ with Ln = La, Ce, Pr, Nd, Sm, and Eu. *J. Solid State Chem.* **2005**, *178*, 72−78.

(33) Nag, A.; Schmidt, P. J.; Schnick, W. Synthesis and Characterization of Tb[N(CN)$_2$]$_3$·2H$_2$O and Eu[N(CN)$_2$]$_3$·2H$_2$O: Two New Luminescent Rare-Earth Dicyanamides. *Chem. Mater.* **2006**, *18*, 5738−5745.

(34) Kelley, S. P.; Rogers, R. D. Isolation of uranyl dicyanamide complexes from N-donor ionic liquids. *Inorg. Chem.* **2015**, *54*, 10323−10334.

(35) MacFarlane, D. R.; Forsyth, S. A.; Golding, J.; Deacon, G. B. Ionic liquids based on imidazolium, ammonium and pyrrolidinium salts of the dicyanamide anion. *Green Chem.* **2002**, *4*, 444−448.

(36) Dieke, G. H.; Crosswhite, H. M.; Crosswhite, H. *Spectra and Energy Levels of Rare Earth Ions in Crystals*; Interscience Publishers, 1968.

(37) Carnall, W.; Crosswhite, H.; Crosswhite, H. M. *Energy Level Structure and Transition Probabilities in the Spectra of the Trivalent Lanthanides in LaF₃*; Argonne National Laboratory (ANL): Argonne, IL, 1978.

(38) *X-RED 1.22, Stoe Data Reduction Program (C)*; Stoe & Cie GmbH: Darmstadt, 2001.

(39) *X-Shape 1.06, Crystal Optimization for Numerical Absorption Correction (C)*; Stoe & Cie GmbH: Darmstadt, 1999.

(40) Sheldrick, G. SHELXT - Integrated space-group and crystal-structure determination. *Acta Crystallogr., Sect. A: Found. Adv.* **2015**, *71*, 3−8.

(41) Sheldrick, G. Crystal structure refinement with SHELXL. *Acta Crystallogr., Sect. C: Struct. Chem.* **2015**, *71*, 3−8.

(42) Spek, A. PLATON SQUEEZE: a tool for the calculation of the disordered solvent contribution to the calculated structure factors. *Acta Crystallogr., Sect. C: Struct. Chem.* **2015**, *71*, 9−18.

(43) Jürgens, B.; Irran, E.; Schnick, W. Syntheses, Vibrational Spectroscopy, and Crystal Structure Determination from X-Ray Powder Diffraction Data of Alkaline Earth Dicyanamides M[N-(CN)₂]₂ with M = Mg, Ca, Sr, and Ba. *J. Solid State Chem.* **2001**, *157*, 241−249.

(44) McCrary, P. D.; Chatel, G.; Alaniz, S. A.; Cojocaru, O. A.; Beasley, P. A.; Flores, L. A.; Kelley, S. P.; Barber, P. S.; Rogers, R. D. Evaluating Ionic Liquids as Hypergolic Fuels: Exploring Reactivity from Molecular Structure. *Energy Fuels* **2014**, *28*, 3460−3473.

(45) Bernardino, K.; Lima, T. A.; Ribeiro, M. C. C. Low-Temperature Phase Transitions of the Ionic Liquid 1-Ethyl-3-methylimidazolium Dicyanamide. *J. Phys. Chem. B* **2019**, *123*, 9418−9427.

(46) Chemistry of Pseudohalides. In *Topics in Inorganic and General Chemistry*; Golub, A. M., Kohler, H., Skopenko, V. V., Eds.; Elsevier: Amsterdam, The Netherlands, 1986; Vol. *21*; pp 434−454.

(47) Reisfeld, R. Spectra and Energy Transfer of Rare Earths in Inorganic Glasses. In *Rare Earths*; Springer, 1973; p 53−98.

(48) Blasse, G.; Grabmaier, B. *Luminescent Materials*; Springer: Berlin, 1994.

(49) Brandner, A.; Kitahara, T.; Beare, N.; Lin, C.; Berry, M. T.; May, P. S. Luminescence Properties and Quenching Mechanisms of Ln(Tf₂N)₃ Complexes in the Ionic Liquid bmpyr Tf₂N. *Inorg. Chem.* **2011**, *50*, 6509−6520.

(50) Mudring, A.-V.; Babai, A.; Arenz, S.; Giernoth, R.; Binnemans, K.; Driesen, K.; Nockemann, P. Strong luminescence of rare earth compounds in ionic liquids: Luminescent properties of lanthanide-(III) iodides in the ionic liquid 1-dodecyl-3-methylimidazolium bis(trifluoromethanesulfonyl)imide. *J. Alloys Compd.* **2006**, *418*, 204−208.